Epitaxial B-Graphene: Large-Scale Growth and Atomic Structure

Dmitry Yu. Usachov,[*,†] Alexander V. Fedorov,[†,‡,§] Anatoly E. Petukhov,[†] Oleg Yu. Vilkov,[†] Artem G. Rybkin,[†] Mikhail M. Otrokov,[⊥,∥] Andrés Arnau,[⊥] Evgueni V. Chulkov,[⊥,∥] Lada V. Yashina,[#] Mani Farjam,[▽] Vera K. Adamchuk,[†] Boris V. Senkovskiy,[†,⊗] Clemens Laubschat,[⊗] and Denis V. Vyalikh[†,⊥,⊗,¶]

[†]Saint Petersburg State University, 198504 St. Petersburg, Russia, [‡]II Physikalisches Institut, Universität zu Köln, Zülpicher Strasse 77, 50937 Köln, Germany, [§]IFW Dresden, P.O. Box 270116, D-01171 Dresden, Germany, [⊥]Donostia International Physics Center (DIPC), Departamento de Fisica de Materiales and CFM-MPC UPV/EHU, 20080 San Sebastian, Spain, [∥]Tomsk State University, Lenina Av., 36, 634050 Tomsk, Russia, [#]M.V. Lomonosov Moscow State University, Leniskie Gory 1/3 199991 Moscow, Russia, [▽]Institute for Research in Fundamental Sciences (IPM), P.O. Box 19395-5531, Tehran, Iran, [⊗]Institute of Solid State Physics, Dresden University of Technology, D-01062 Dresden, Germany, and [¶]IKERBASQUE, Basque Foundation for Science, 48011 Bilbao, Spain

ABSTRACT Embedding foreign atoms or molecules in graphene has become the key approach in its functionalization and is intensively used for tuning its structural and electronic properties. Here, we present an efficient method based on chemical vapor deposition for large scale growth of boron-doped graphene (B-graphene) on Ni(111) and Co(0001) substrates using carborane molecules as the precursor. It is shown that up to 19 at. % of boron can be embedded in the graphene matrix and that a planar C—B sp^2 network is formed. It is resistant to air exposure and widely retains the electronic structure of graphene on metals. The large-scale and local structure of this material has been explored depending on boron content and substrate. By resolving individual impurities with scanning tunneling microscopy we have demonstrated the possibility for preferential substitution of carbon with boron in one of the graphene sublattices (unbalanced sublattice doping) at low doping level on the Ni(111) substrate. At high boron content the honeycomb lattice of B-graphene is strongly distorted, and therefore, it demonstrates no unballanced sublattice doping.

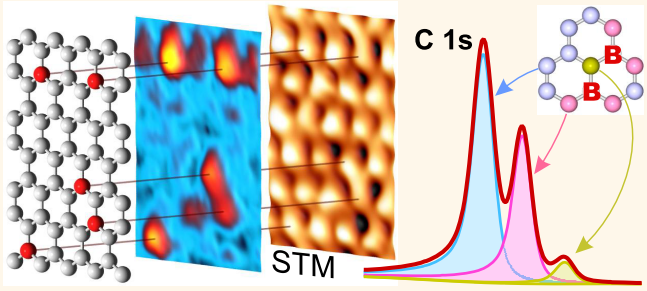

KEYWORDS: graphene · boron · doping · electronic structure · photoemission spectroscopy · tunneling microscopy

Graphene functionalization is a rapidly developing area of research focused at graphene modification for making this unique 2D material essential for a broad variety of applications.[1,2] Among the multiple developed approaches, incorporation of impurities in graphene is shown to be an efficient and versatile method for controllable tuning of its physical and chemical properties.[3−7] For example, by substituting carbon atoms with nitrogen or boron,[8] it is possible to turn graphene into a semiconductor of *n*- or *p*-type, respectively.[9] Such impurity-related modifications of electronic structure and physicochemical properties greatly extend capabilities of the doped graphene use in nanoelectronics, in oxygen reduction reactions occurring in fuel cells, batteries, supercapacitors and many other applications.[6,10] Currently it is well-understood that the doped graphene characteristics are governed by not only the type of guest atoms, but also by the local structure of impurities.[11−13] Therefore, detailed structural characterization is a key point for understanding and precise controlling of the properties of this material.

As compared to nitrogen,[3] boron can be embedded in graphene at higher concentrations[14−16] that gives broader opportunities to tune its properties. This makes boron-doped graphene (B-graphene) a unique and very attractive material from both fundamental and practical viewpoints. Experimental study of the electronic structure of B-graphene revealed a *p*-type doping effect.[17] However, for such a system its structural organization from large scale to local environment of foreign atoms is currently not well-known, and it is in the focus of the present work. The structure of B-graphene is governed by the synthesis method and conditions, and postgrowth treatment as well. One of the most efficient

* Address correspondence to usachov.d@gmail.com.

Received for review April 15, 2015 and accepted June 29, 2015.

Published online June 29, 2015
10.1021/acsnano.5b02322

methods for the doped graphene synthesis is a chemical vapor deposition (CVD), which has become a key method for large-scale graphene growth on a wide variety of substrates.[18] The structure and catalytic activity of the substrate play a significant role in the CVD process and have a great impact on the structure of the obtained graphene-based system. Recent studies of nitrogen-doped graphene[19,20] have demonstrated that the Ni(111) surface is a very convenient substrate for the synthesis of doped graphene, tuning of its electronic structure and controlling the bonding configurations of the nitrogen impurities. One of the reasons for that is an almost perfect matching of the lattice constants that promotes formation of a high-quality well oriented layer with a (1 × 1) structure at certain conditions of the synthesis procedure. The same property was recently reported for the case of boron-doped graphene on Ni(111), too.[14] A uniform orientation of graphene domains allows to accurately explore the electronic landscape of this system with angle-resolved photoemission spectroscopy (ARPES).[14] However, a well-known strong hybridization between the graphene Dirac cone states and 3*d* orbitals of nickel[21] is an important issue that hampers the studies of dopant-related electronic modifications in B-graphene. This strong interaction can be eliminated by intercalation of guest atoms in the graphene/nickel interface. One of the most efficient materials used for such decoupling is gold, because its 5*d* states are filled and energetically shifted away from the Fermi level (E_F), and therefore are less active chemically. Gold weakly interacts with graphene and provides negligible charge transfer.[22,23] We have recently shown that gold intercalation can be easily achieved in the case of pure and N-doped graphene/Ni(111).[23] However, it was demonstrated to be not efficient in the case of B-graphene/Ni(111) interface.[14,15] Thus, ARPES studies of the electronic structure of intercalated quasi-freestanding B-graphene remain a challenge.

The other potentially useful property of the graphene/Ni(111) interface is a broken symmetry of the two carbon sublattices in the (1 × 1) structure. Energetically, the most favorable configuration is achieved when the carbon atoms of one sublattice are positioned right above the Ni atoms, while those of the other sublattice are located above the hollow sites.[24] It is therefore natural to expect that the probability of impurity incorporation in graphene during CVD synthesis on the Ni(111) surface will be different for the two sublattices. In this case one may hope to obtain a graphene layer with impurities, which substitute the carbon atoms of preferably one sublattice. It has been theoretically demonstrated that such unbalanced sublattice doping[25,26] should lead to opening of a valuable gap in the Dirac cone spectrum.[5,25] After being transferred to an insulating substrate this kind of doped graphene may be of a great interest for electronic applications as a unique semiconducting 2D material. The prediction of a gap is consistent with our ARPES study of N-graphene, grown on Ni(111),[7] but transport measurements are still required to provide indisputable evidence. In the case of B-graphene/SiO_2 the transport studies revealed notable band gap, depending on the boron concentration,[27] but the origin of the gap is not clear in view of ref 5.

It should be noticed that there is another surface, which is very similar to Ni(111) regarding its crystal structure and properties, namely Co(0001). Graphene can be easily grown on this substrate,[28] and a (1 × 1) structure can be obtained at certain conditions;[29,30] however, no studies of doped graphene on this type of surface have been reported yet.

In this work we present a comprehensive study of the B-graphene/Ni(111) system applying a set of local and nonlocal techniques. We have found strong evidence for a substitutional type of doping and established conditions for preferential substitution of carbon in one of the graphene sublattices (unbalanced sublattice doping), which opens a way to control the electronic structure of this 2D material. Moreover, this work demonstrates the CVD synthesis of B-graphene on the Co(0001) surface and characterization of its properties and provides a detailed comparison with the case of the Ni(111) substrate.

RESULTS AND DISCUSSION

B-graphene was synthesized by CVD from the mixture of carborane and propylene, according to the procedure, described in the section Methods. Figures 1a,b show XPS spectra of B-graphene/Ni(111) samples with different boron concentrations. The C 1*s* XPS spectrum consists of three components C_0, C_1, C_2 with notably different binding energies (BE), indicating different local environments of the respective C atoms. The BE of the most intensive component C_0 notably depends on the boron concentration. However, at small doping it is approaching the C 1*s* BE value of the pure graphene on the Ni(111) surface, marked with the dashed line at 284.95 eV. It allows to conclude that the peak C_0 corresponds to the carbon atoms, surrounded by three carbon neighbors. The intensities of the C_1 and C_2 components are rising when the boron concentration is increased. It allows to assign these peaks to carbon atoms, which form bonds with boron atoms. The nature of these bonds will be discussed further.

The upper B 1*s* spectrum in Figure 1b corresponds to B-graphene, which was synthesized from pure carborane and has maximal boron concentration (19 at. %). This spectrum consists of two components B_0 and B_1. According to our XPS data, acquired at different photon energies (see Figure S2 and related discussion in Supporting Information), the narrow peak B_0 with the BE of 188 eV corresponds to boron atoms under the B-graphene layer. These boron atoms are preferably located in the bulk of the Ni film. Also crystalline nickel boride is formed at the Ni(111) surface, as it is

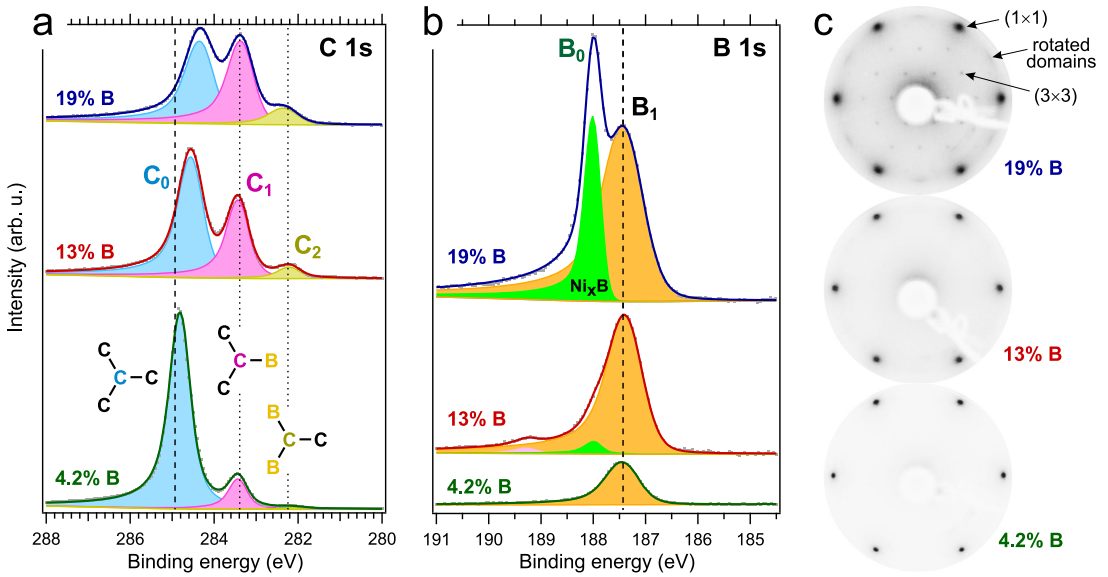

Figure 1. (a,b) XPS spectra of B-graphene/Ni(111) systems with different boron concentration. The spectra were acquired at a photon energy of 380 eV. (c) Corresponding LEED patterns, obtained with an electron beam energy of 70 eV.

evidenced by the appearance of a (3 × 3) superstructure in the upper LEED pattern in Figure 1c and a (3 × 3) moiré structure in the STM images of B-graphene (see Figure S3, S4 in Supporting Information). At lower boron concentrations, when carborane was mixed with propylene during synthesis, the formation of nickel boride was strongly suppressed. This can be explained by a higher rate of graphene growth in the presence of propylene. Also no segregation of boron from the Ni film was detected upon further annealing of B-graphene/Ni(111) systems at temperatures below 600 °C. At low boron content (4.2 at. %) the B 1*s* spectrum consists of a single peak B_1 at 187.4 eV. In some cases we observed an additional component at 189.3 eV (see the middle spectrum in Figure 1b); however, its intensity was always negligible with respect to the main peak.

At low boron concentration, when boron atoms are supposed to form single impurities, it is possible to determine the stoichiometry of boron-related defects. Figure 1a shows that at 4.2 at. % of boron the peak C_1 exhibits notable intensity, while the peak C_2 is hardly visible. If we neglect the peak C_2 and assume that all boron atoms are bonded to carbon atoms of the peak C_1, it is easy to calculate how many carbon atoms are bonded to a single boron impurity. This follows from the intensity ratio of C_1 and B_1 peaks (see section Methods for further details). The analysis shows that boron is bonded to three carbon neighbors. This corresponds to a situation, when boron substitutes carbon in the graphene lattice. The XPS binding energies for the case of substitutional doping were calculated in ref 14, and it was shown that the BE of the C_1 peak corresponds to the case when a carbon atom has two C neighbors and one B neighbor ($C{-}C_2B$ environment). The peak C_2 was assigned to a $C{-}B_2C$ structure with two B neighbors. Further we will show that such assignment of the peak C_2 is confirmed by our analysis of XPS intensities.

The macroscopic structure of the B-graphene layer is reflected in the LEED images, presented in Figure 1c. At low boron content the diffraction pattern represents a nice hexagon. It means that B-graphene is well oriented and forms a (1 × 1) structure. However, with increasing boron concentration the arc-shaped reflexes appear in the LEED pattern. They become very prominent at maximal doping and indicate the presence of misoriented B-graphene domains. The background intensity is also enhanced at high boron concentrations. It reflects the amount of impurities and other defects, which lead to incoherent electron scattering.

The strong evidence that boron is incorporated in a planar graphene lattice comes from NEXAFS data. Figures 2a,b show the dependence of X-ray absorption spectra on the angle between the surface and the polarization vector of the linearly polarized radiation. The absorption cross section, which corresponds to electron transition from 1*s* to 2*p* orbitals, is proportional to the projection of the polarization vector on the *p*-orbital axis. Thus, for $2p_z$ orbitals, which form π bonds, the absorption vanishes at zero angle. For σ bonds, which are perpendicular to the π bonds, the absorption reaches maximum. Such behavior is a good indicator of planar sp^2 structure. For pure sp^3 configuration no angular dependence is expected. It can be seen from Figure 2a,b that both carbon and boron K-edges demonstrate angular dependence, typical for sp^2 structures. Thus, we can conclude that boron and carbon form a planar sp^2 system. In the case of maximal boron concentration the spectra at the boron K-edge show weak angular dependence due to a dominating signal from the nickel boride, which is formed under B-graphene. At lower boron concentrations the spectra

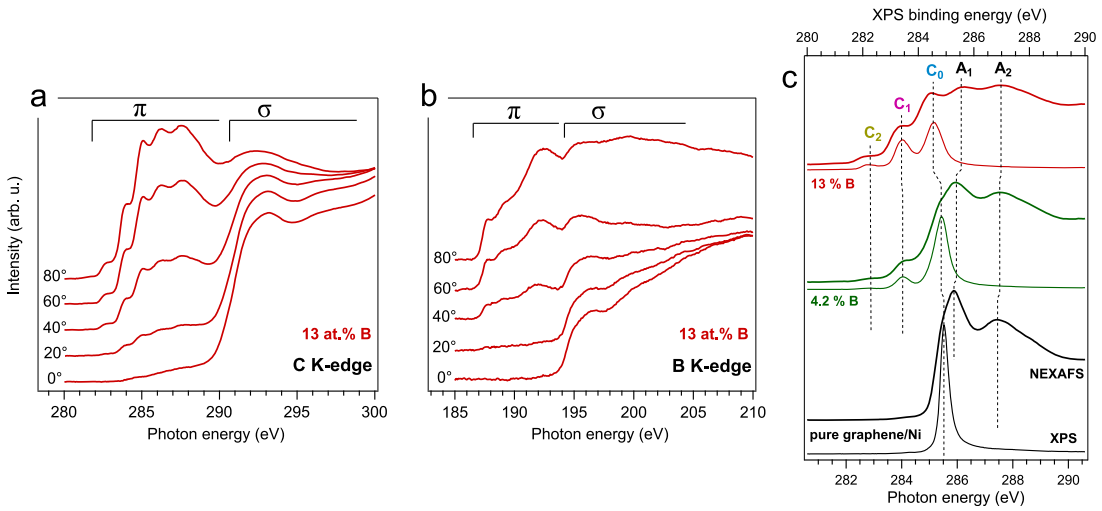

Figure 2. (a,b) Angular dependence of B-graphene/Ni(111) NEXAFS spectra at boron concentration of 13 at. %. (c) Comparison of the K-edge carbon NEXAFS spectra, acquired at the angle of 80°, with the C 1*s* XPS spectra of B-graphene at different boron concentrations.

demonstrate nice sp^2 structures, although the shape of the spectra depends on the doping level. This dependence is presented in Figure 2c. The shape of the carbon K-edge spectrum becomes more complicated with increasing boron content. Instead of a single sharp absorption edge of undoped graphene we can see three features C_0, C_1, C_2. The intensity and energy of these features correlate with the parameters of the three peaks in C 1*s* XPS spectra. Thus, the features can be directly assigned to the different local environments of the carbon atoms. The features A_1 and A_2 are related to a specific electronic structure of the unoccupied π states of pure and B-graphene.

To gain deeper understanding of the B-graphene crystal structure we performed STM studies with atomic resolution of the B-graphene/Ni(111) system with 3.7 at. % of boron. This concentration is low enough for resolving individual impurities. We have found that overwhelming part of the surface is covered by a (1 × 1) B-graphene lattice, in accordance with the LEED data; however, in some regions one can find rotated domains of different sizes. In the upper part of Figure 3a there is an example of small rotated grain, consisting of few B-graphene rings, shown with yellow hexagons. The rotated domain is incorporated into a (1 × 1) domain, shown with white hexagons. The two domains are connected with the grain boundary, consisting of five- and seven-member rings, similarly to the grain boundaries in pure graphene.[24,31,32] In the STM image of a (1 × 1) domain there is a notable asymmetry between the two different sublattices due to influence of the Ni(111) surface atoms. Simulations of the graphene/Ni(111) STM images[24,33] demonstrate that the sublattice H, which is located above the hollow sites of the Ni(111) surface (see Figure 3b), must appear higher than the sublattice T, located above the Ni atoms. This allows us to determine the positions of the topmost Ni atoms in the STM images (see blue circles in Figure 3a).

In the lower part of Figure 3a the boundary between larger rotated domain and (1 × 1) domain is marked out. The rotated B-graphene lattice is incommensurate to the Ni(111) surface, therefore, there is no regular asymmetry between the two sublattices and the STM image demonstrates a honeycomb structure, although it is slightly distorted by the interaction with the substrate. Another characteristic feature of the B-graphene topography shown in Figure 3a is a presence of multiple triangular depressions, which could be associated with boron impurities. This interpretation is consistent with the simulated STM image of B-graphene, shown in Figure 3b. The triangular shape of impurities is typical for STM images of doped graphene,[34−37] however, in the B-graphene/Ni(111) system the impurities appear not as prominent as, for example, in B-graphene on copper.[34]

Since constant-current STM images have not revealed prominent contrast between carbon and boron atoms in atomically resolved data, we applied a current imaging tunneling spectroscopy (CITS), in which the tunneling current is recorded as a function of voltage in each point of the STM image. The current is nearly proportional to the sample local density of states (LDOS), integrated in the energy range between the E_F and the bias voltage.[38] Therefore, the derivative dI_t/dV_t reflects the LDOS at electron energy corresponding to the selected bias voltage. Since boron and carbon have a different LDOS, the contrast can be observed at certain bias.[36] The obtained results are shown in Figure 4. The first panel shows a constant-current STM image of the (1 × 1) domain, where boron impurities are hardly distinguishable. The corresponding CITS image, which reflects the LDOS at the energy of 0.2 eV below the E_F, is shown in Figure 4b. It reveals point defects with lower LDOS. The concentration of these defects is 4 ± 1 at. %, which is consistent with the boron concentration, measured with XPS (3.7 at. %).

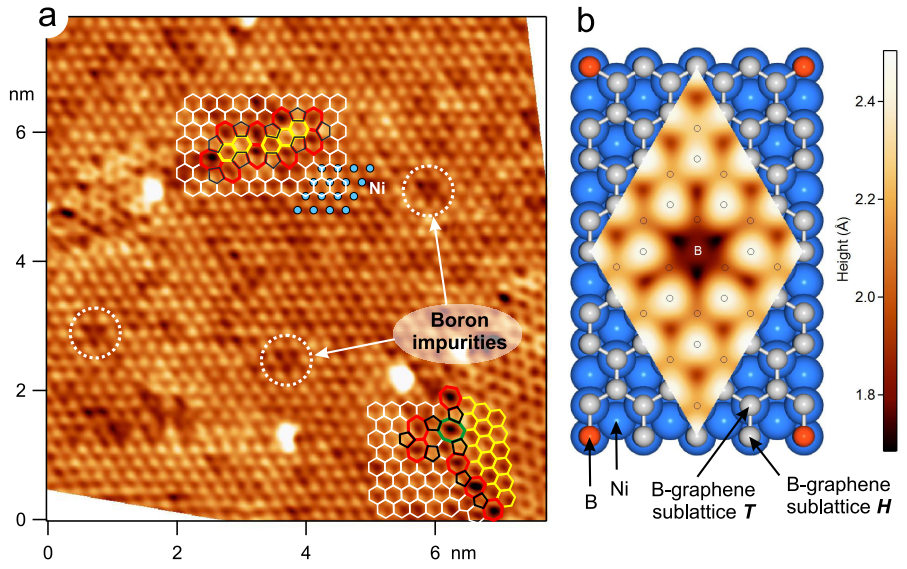

Figure 3. (a) Constant-current STM image of B-graphene/Ni(111) with boron concentration of 3.7 at. %. The image was obtained at sample bias $V_t = 2$ mV and current $I_t = 1.8$ nA. Light tones correspond to higher regions. (b) The structural model of a (1 × 1) B-graphene domain and superimposed simulated STM image (see Supporting Information for calculation details). Open circles indicate carbon atoms.

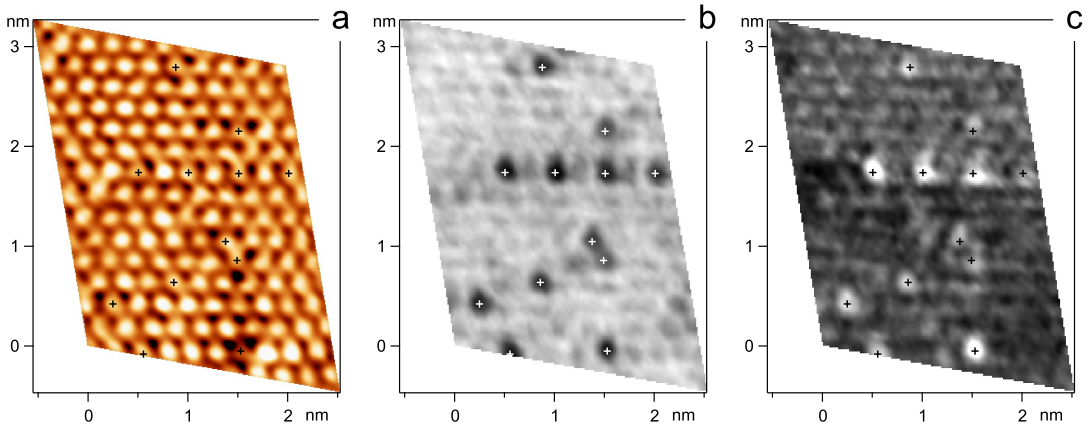

Figure 4. (a) Constant-current STM image of B-graphene/Ni(111) at boron concentration of 3.7 at. %. Sample bias voltage was $V_t = 6$ mV at tunneling current value $I_t = 2.2$ nA. (b,c) Corresponding CITS images, showing dI_t/dV_t maps at the sample bias voltage of (b) $V_t = -0.2$ V and, (c) $V_t = +0.2$ V, which correspond to LDOS below and above E_F, accordingly. Light tones correspond to higher values of height or dI_t/dV_t. Crosses show locations of boron impurities.

This fact allows us to directly relate the observed defects to the boron impurities. The CITS image, corresponding to the LDOS above the E_F (Figure 4c), reveals the same point defects; however, their LDOS appears higher, than that at the rest of the surface. From the comparison between CITS and STM images we can conclude, that the observed boron impurities are all embedded in the sublattice H, which is located above the hollow sites of the Ni(111) surface (see Figure 3b). This result is in agreement with the recent calculation,[14] which predicted that these sites are energetically most favorable for boron substitutions in graphene/Ni(111) system. Our *ab initio* calculations (see Supporting Information) also confirm that the hollow sites are more favorable than the top sites. In order to support the conclusion that the contrast observed in CITS can be related to boron impurities we have calculated the LDOS of B-graphene/Ni(111) system with 3.1 at. % of boron. The results demonstrate that in the energy region from 0 to 0.3 eV (above the E_F) the LDOS at the boron location is lower, than the LDOS at any carbon atom site (see Figure S10 in Supporting Information). At higher energies from 0.4 to 0.5 eV the contrast is reversed and the LDOS at the boron site appears higher. This is in agreement with the CITS results if one considers an energy shift of 0.25 eV. The possible reason for such a discrepancy is 2-fold. First, the STM and CITS images are known to be substantially dependent on the tip geometry and electronic structure, which are not taken into account in our simulation. Second, since density functional theory is based on certain approximations, it is natural that the calculated

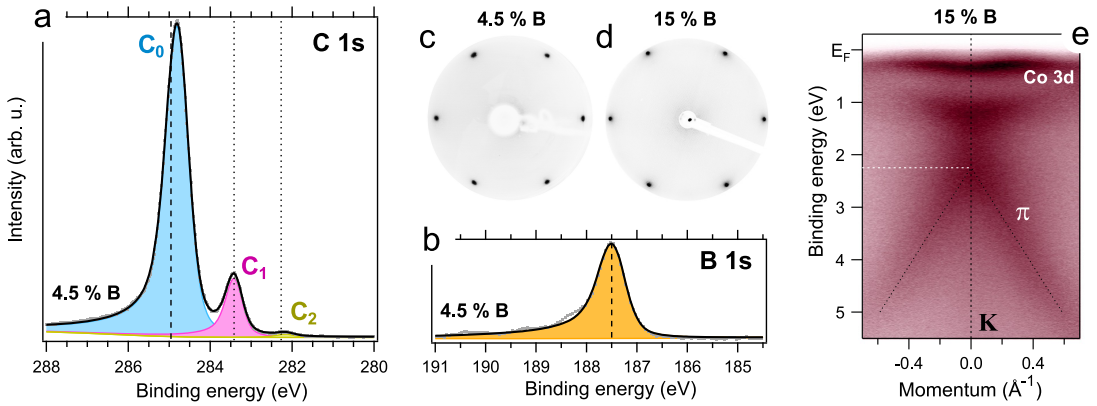

Figure 5. B-graphene/Co(0001) system: (a,b) XPS spectra at 4.5 at. % of boron impurities, measured at photon energy of 380 eV, (c,d) LEED images, obtained at different boron content using electron energy of 70 eV, (e) ARPES spectrum at 15 at. % B, recorded near the K-point of the two-dimensional Brillouin zone in the direction, perpendicular to ΓK. Dashed line in panel (a) indicates C 1*s* BE value of the pure graphene/Co(0001).

band energies differ somewhat from the measured ones. Typically, the agreement between the theory and experiment is about 0.1−0.3 eV for crystalline solids. For example, the discrepancies between measured and calculated spectral features of graphene on metallic substrates can reach several hundred meV even in the undoped graphene case.[28,30,39] Thus, we are convinced that the point defects, detected in the CITS images, originate from boron impurities.

Production of doped graphene with impurities occupying predominantly one sublattice is of great importance for possible electronic applications of B-graphene. Among our samples only well-oriented (1 × 1) graphene at relatively small boron concentrations (up to ~5 at. %) may be a good candidate for achieving a band gap, induced by sublattice asymmetry of doping. At concentrations higher than 12 at. % B-graphene is not well-ordered and consists of plenty of misoriented domains. In this case no preferred sublattice is expected for boron impurities due to the incommensurate structure of the B-graphene/Ni(111) system. Here the following question arises: if it would be possible to find appropriate conditions for the formation of well-oriented B-graphene with high dopant concentration, should we necessarily observe the sublattice asymmetry of doping? In order to answer this question we have tried to achieve better orientation of B-graphene at high boron concentration by using the Co(0001) surface.

For the synthesis of B-graphene on cobalt we have used the same CVD procedure with carborane and propylene, as it was elaborated for the nickel substrate (see section Methods). XPS spectra of B-graphene/Co(0001) system, shown in Figure 5a,b are similar to the spectra of B-graphene/Ni(111) and can be interpreted in the same way. The LEED patterns, obtained at different boron content, indicate that the system remains well-oriented for impurity concentrations up to 15 at. %. The presence of misoriented domains is hardly detectable; it can be seen only at very enhanced image contrast. Nevertheless, STM images demonstrate that in spite of nice LEED pattern the crystal structure of B-graphene at 15 at. % of boron is far from perfection. The honeycomb lattice is strongly distorted and contains multiple defects (see Figure S8 in Supporting Information). Surprisingly, heavily doped layers retain the electronic structure, similar to pure graphene/metal system. This is evidenced by presence of a Dirac cone in the ARPES data, shown in Figure 5e. The conical structure of the graphene π states is clearly visible at binding energies higher than 2.5 eV. In the region of 0−2.5 eV the Dirac cone is destroyed by hybridization of graphene states with Co 3*d* states, which is typical for single-layer graphene.[21,23,40] The only difference from the undoped graphene is an energy shift of the π band toward the E_F by ~0.5 eV (see Figure S6 in Supporting Information). This shift is caused by impurities and it is a good indicator that boron atoms are distributed homogeneously within the graphene lattice; *i.e.*, no undoped graphene regions are present in the system.

As we have shown, STM is efficient for detecting impurity sites at low concentrations. At high amount of boron the structure is hardly resolved, therefore we have developed a method for testing sublattice asymmetry of doping with XPS. Figure 6 shows the evolution of intensities of the three peaks in C 1*s* XPS spectra (see Figure 1a) as a function of boron concentration. The experimental values, determined for several B-graphene samples, are shown with circles and triangles. In order to describe the obtained dependence we considered two models of the B-graphene structure. In the first model we assumed that boron impurities randomly substitute carbon atoms in the two graphene sublattices. In the second model we allowed substitution only in one sublattice (see Figure S5 in Supporting Information). Additionally, in accordance with the XPS spectra analysis we suggested that boron dopants can be surrounded by three carbon neighbors, while carbon atoms may have three types of nearest coordination spheres: C_3, C_2B and B_2C.

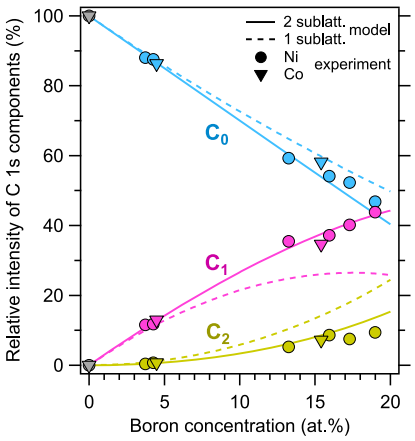

Figure 6. Concentration of carbon atoms with different number of boron neighbors as a function of boron content in B-graphene on Ni(111) and Co(0001) surfaces.

In frames of each model we calculated statistically the number of carbon atoms in different local environment as a function of boron concentration. The results are shown in Figure 6 by solid and dashed lines for the first and second model, respectively. Obviously, differences between the proposed models are experimentally indistinguishable at low boron concentrations (below 6 at. %). At high boron content the model with unbalanced sublattice doping strongly deviates from experiment, while the model with random substitutions in two sublattices perfectly fits experimental data both for Ni(111) and Co(0001) substrates. This leads to several important consequences. First, the presented analysis provides a strong support for the conclusion, that boron atoms substitute carbon in the lattice and the peaks, observed in C 1*s* spectra, indeed correspond to C_3, C_2B and B_2C environments. Second, in spite of good orientation of B-graphene on Co(0001) and predominant (1 × 1) structure in the LEED pattern, no sublattice asymmetry of doping is detected by XPS for 15 at. % of boron. In other words, at high boron concentration impurities occupy any lattice sites with similar probability and the good matching of graphene and substrate lattice parameters and predominant orientation are not sufficient conditions for doping asymmetry. To obtain the latter, the interface structure must be of high quality, which is achieved only at small doping level.

Finally, we should note that for practical applications of B-graphene its stability in contact with air is of high importance. Therefore, we have measured the influence of ambient conditions on B-graphene/Ni(111) system, that is reflected in the XPS spectra. The sample with 16 at. % of boron was exposed to air for ~30 min at relative humidity of ~40%. After that, XPS spectra revealed presence of oxygen and extra carbon adsorbed on the surface. This is typical for any sample after having being exposed to air. After further annealing of B-graphene at a temperature of 550 °C in UHV the shape of the C 1*s* and B 1*s* spectra was almost completely restored (see Figure S9 in Supporting Information), while the oxygen concentration on the surface dropped below 1 at. %. These results indicate stability of B-graphene samples in air and promote future use of this material in variety of graphene-based applications.

CONCLUSIONS

In summary, we have demonstrated an efficient synthesis of single-layer boron-doped graphene on Ni(111) and on Co(0001) surfaces using carborane molecules. By applying a broad variety of surface-sensitive methods (XPS, LEED, ARPES, NEXAFS, STM and CITS) we have studied the structure of boron impurities, incorporated in graphene during CVD synthesis. It has been found that impurities substitute carbon atoms in the graphene lattice and affect the orientation of graphene domains. In the case of the Ni(111) substrate B-graphene is well-oriented at low boron concentrations (<5 at. %). For this kind of sample we observed a strong asymmetry of doping between the two graphene sublattices. STM and CITS data point out that boron atoms occupy preferably lattice sites, located above the hollow sites of the Ni(111) surface. At high doping level (>12 at. %) B-graphene becomes poorly ordered with no sublattice asymmetry. According to the LEED data, B-graphene on the Co(0001) surface may be grown better oriented on the large scale for boron concentrations up to 15 at. %; however, STM shows that its honeycomb lattice is strongly distorted on atomic scale, similarly to the B-graphene/Ni(111). In order to analyze sublattice asymmetry in such strongly doped graphene we have developed an asymmetry-testing method based on XPS spectra. It was found that the B-graphene/Co system shows no doping asymmetry at high boron concentration. Our results clearly demonstrate that strong doping asymmetry in B-graphene on Ni(111) and Co(0001) substrates should be expected only in the case of low dopant concentration. These results represent an important step for further direct transport-based observation of dopant-induced band gap in graphene, which may force further progress in applications of graphene in next-generation electronic devices.

METHODS

Single-layer boron-doped graphene was synthesized by CVD on the surfaces of crystalline Ni(111) and Co(0001) films with the thickness of ~10 nm, grown on a clean W(110) surface in UHV conditions. For the synthesis we used the following procedure. First, the substrate was heated up to 600−630 °C in UHV. Then carborane[41] ($C_2B_{10}H_{12}$) was introduced into the vacuum chamber through the short gas inlet line (length ~10 cm), preliminarily pumped until the pressure was better than

10^{-6} mbar. The carborane source was purified by pumping it with turbomolecular pump before use. Decomposition of carborane molecules on the hot nickel surface resulted in chemisorption of boron and carbon. The amount of boron was controlled by the pressure of carborane, which was in the range of 10^{-8} to 10^{-6} mbar, and by the exposure time (3−20 min). Maximal exposure allowed growth of B-graphene with a boron concentration of 19 at. % on the Ni(111) surface. In order to obtain lower boron concentration in B-graphene we reduced the pure carborane exposure and introduced propylene (C_3H_6) into the chamber (additionally to carborane). The total pressure during the synthesis was 10^{-6} mbar, while the total duration was 20 min for all samples. We suppose the following growth mechanism. At the temperature of synthesis the diffusion of boron in the metal film is quite slow, therefore boron is mainly adsorbed on the surface during the first minutes of synthesis and the amount of boron is expected to be proportional to the carborane exposure. Rapid graphene growth starts when the surface is exposed to propylene after 3 min of carborane exposure. The synthesis reaction is assisted by catalytically active metal and involves chemisorbed boron atoms, which become embedded in the graphene lattice. It is well-known that at the synthesis temperature the graphene growth is limited by formation of a single layer,[42] because no further carbon and boron chemisorption is possible on the graphene-passivated surface. Also no carbon segregation from the metal film occurs after synthesis, because carbon solubility and diffusion rate at the temperature of 600−630 °C are too low. The resulting concentration of boron, embedded in B-graphene, is defined by the amount of initially chemisorbed boron, controlled by the carborane pressure. When B-graphene is grown solely from carborane the growth rate is slow due to lack of carbon, therefore there is enough time for boron to diffuse into bulk. This synthesis mechanism differs from the growth of N-graphene/Ni(111), where most of the chemisorbed nitrogen is desorbed during the synthesis and only a small fraction is embedded in graphene.[7] It also differs from the approach used in ref 19, where B-graphene growth on nickel was accompanied by precipitation of boron, preliminary dissolved in the bulk.

XPS measurements were performed at the Resource Center "Physical Methods of Surface Investigation" (RC PMSI) of Research park of Saint Petersburg State University and at the Russian-German beamline (RGBL) of BESSY II synchrotron radiation facility. The samples were studied in the same UHV system where they were synthesized. Boron and carbon concentrations were carefully evaluated from the intensity ratio of C 1*s* and B 1*s* lines in XPS spectra, recorded with Scienta R4000 electron analyzer in the RC PMSI using monochromated Al Kα radiation (see Figure S1 in Supporting Information). For this purpose the spectra were corrected for analyzer transmission function, provided by manufacturer (although this correction is only few %). Also we took into account inelastic photoelectron scattering within the B-graphene layer (see Supporting Information). In order to evaluate concentrations from the spectra, measured with photon energy of 380 eV at RGBL, we have applied atomic sensitivity factors, determined using the reference B-graphene sample, preliminarily characterized in RC PMSI and transferred to RGBL in the argon atmosphere.

STM and CITS images were obtained at the room temperature using Omicron VT SPM in RC PMSI. The microscope is located in the same UHV system, where the B-graphene was synthesized and characterized with photoelectron spectroscopy; thus, the samples were not exposed to air before STM measurements.

NEXAFS data were obtained at RGBL by measuring total electron yield.

Conflict of Interest: The authors declare no competing financial interest.

Acknowledgment. The authors acknowledge Saint Petersburg State University for Research Grants 11.37.634.2013 and 11.50.202.2015, RFBR (Grant No. 14-02-31150), and BMBF (Grant No. 05K12OD3). We acknowledge Helmholtz Zentrum Berlin für Materialien und Energie for support within bilateral Russian-German Laboratory program. MMO and EVC acknowledge the Tomsk State University Academic D.I. Mendeleev Fund Program (Research Grant No. 8.1.05.2015). *Ab initio* calculations were performed on the SKIF-Cyberia supercomputer of Tomsk State University. We cordially thank Prof. V.I. Bregadze for consultations on boron organic chemistry and the provision of carborane.

Supporting Information Available: Additional results of the XPS, ARPES, STM and DFT studies are presented. The Supporting Information is available free of charge on the ACS Publications website at DOI: 10.1021/acsnano.5b02322.

REFERENCES AND NOTES

1. Craciun, M.; Khrapach, I.; Barnes, M.; Russo, S. Properties and Applications of Chemically Functionalized Graphene. *J. Phys.: Condens. Matter* **2013**, *25*, 423201.
2. Mao, H. Y.; Lu, Y. H.; Lin, J. D.; Zhong, S.; Wee, A. T. S.; Chen, W. Manipulating the Electronic and Chemical Properties of Graphene *via* Molecular Functionalization. *Prog. Surf. Sci.* **2013**, *88*, 132–159.
3. Wang, H.; Maiyalagan, T.; Wang, X. Review on Recent Progress in Nitrogen-Doped Graphene: Synthesis, Characterization, and Its Potential Applications. *ACS Catal.* **2012**, *2*, 781–794.
4. Paek, E.; Pak, A. J.; Kweon, K. E.; Hwang, G. S. On the Origin of the Enhanced Supercapacitor Performance of Nitrogen-Doped Graphene. *J. Phys. Chem. C* **2013**, *117*, 5610–5616.
5. Lherbier, A.; Botello-Méndez, A. R.; Charlier, J.-C. Electronic and Transport Properties of Unbalanced Sublattice N-Doping in Graphene. *Nano Lett.* **2013**, *13*, 1446–1450.
6. Yu, Y.-X. Can All Nitrogen-Doped Defects Improve the Performance of Graphene Anode Materials for Lithium-Ion Batteries? *Phys. Chem. Chem. Phys.* **2013**, *15*, 16819–16827.
7. Usachov, D.; Vilkov, O.; Grüneis, A.; Haberer, D.; Fedorov, A.; Adamchuk, V. K.; Preobrajenski, A. B.; Dudin, P.; Barinov, A.; Oehzelt, M.; *et al.* Nitrogen-Doped Graphene: Efficient Growth, Structure, and Electronic Properties. *Nano Lett.* **2011**, *11*, 5401–5407.
8. Rao, C.; Gopalakrishnan, K.; Govindaraj, A. Synthesis, Properties and Applications of Graphene Doped with Boron, Nitrogen and Other Elements. *Nano Today* **2014**, *9*, 324–343.
9. Lherbier, A.; Blase, X.; Niquet, Y.-M.; Triozon, F.; Roche, S. Charge Transport in Chemically Doped 2D Graphene. *Phys. Rev. Lett.* **2008**, *101*, 036808.
10. Sahoo, N. G.; Pan, Y.; Li, L.; Chan, S. H. Graphene-Based Materials for Energy Conversion. *Adv. Mater.* **2012**, *24*, 4203–4210.
11. Schiros, T.; Nordlund, D.; Pálová, L.; Prezzi, D.; Zhao, L.; Kim, K. S.; Wurstbauer, U.; Gutiérrez, C.; Delongchamp, D.; Jaye, C.; *et al.* Connecting Dopant Bond Type with Electronic Structure in N-Doped Graphene. *Nano Lett.* **2012**, *12*, 4025–4031.
12. Kondo, T.; Casolo, S.; Suzuki, T.; Shikano, T.; Sakurai, M.; Harada, Y.; Saito, M.; Oshima, M.; Trioni, M. I.; Tantardini, G. F.; *et al.* Atomic-Scale Characterization of Nitrogen-Doped Graphite: Effects of Dopant Nitrogen on the Local Electronic Structure of the Surrounding Carbon Atoms. *Phys. Rev. B: Condens. Matter Mater. Phys.* **2012**, *86*, 035436.
13. Hou, Z.; Wang, X.; Ikeda, T.; Terakura, K.; Oshima, M.; Kakimoto, M.-a. Electronic Structure of N-Doped Graphene with Native Point Defects. *Phys. Rev. B: Condens. Matter Mater. Phys.* **2013**, *87*, 165401.
14. Gebhardt, J.; Koch, R. J.; Zhao, W.; Höfert, O.; Gotterbarm, K.; Mammadov, S.; Papp, C.; Görling, A.; Steinrück, H.-P.; Seyller, T. Growth and Electronic Structure of Boron-Doped Graphene. *Phys. Rev. B: Condens. Matter Mater. Phys.* **2013**, *87*, 155437.
15. Zhao, W.; Gebhardt, J.; Gotterbarm, K.; Höfert, O.; Gleichweit, C.; Papp, C.; Görling, A.; Steinrück, H.-P. Gold Intercalation of Boron-Doped Graphene on Ni(111): XPS and DFT Study. *J. Phys.: Condens. Matter* **2013**, *25*, 445002.
16. Yen, W.-C.; Medina, H.; Huang, J.-S.; Lai, C.-C.; Shih, Y.-C.; Lin, S.-M.; Li, J.-G.; Wang, Z. M.; Chueh, Y.-L. Direct Synthesis of

Graphene with Tunable Work Function on Insulators via In Situ Boron Doping by Nickel-Assisted Growth. *J. Phys. Chem. C* **2014**, *118*, 25089–25096.
17. Cattelan, M.; Agnoli, S.; Favaro, M.; Garoli, D.; Romanato, F.; Meneghetti, M.; Barinov, A.; Dudin, P.; Granozzi, G. Microscopic View on a Chemical Vapor Deposition Route to Boron-Doped Graphene Nanostructures. *Chem. Mater.* **2013**, *25*, 1490–1495.
18. Wu, T.; Shen, H.; Sun, L.; Cheng, B.; Liu, B.; Shen, J. Nitrogen and Boron Doped Monolayer Graphene by Chemical Vapor Deposition Using Polystyrene, Urea and Boric Acid. *New J. Chem.* **2012**, *36*, 1385–1391.
19. Koch, R. J.; Weser, M.; Zhao, W.; Viñes, F.; Gotterbarm, K.; Kozlov, S. M.; Höfert, O.; Ostler, M.; Papp, C.; Gebhardt, J.; *et al.* Growth and Electronic Structure of Nitrogen-Doped Graphene on Ni(111). *Phys. Rev. B: Condens. Matter Mater. Phys.* **2012**, *86*, 075401.
20. Usachov, D.; Fedorov, A.; Vilkov, O.; Senkovskiy, B.; Adamchuk, V.; Yashina, L.; Volykhov, A.; Farjam, M.; Verbitskiy, N.; Grüneis, A.; *et al.* The Chemistry of Imperfections in N-Graphene. *Nano Lett.* **2014**, *14*, 4982–4988.
21. Grüneis, A.; Vyalikh, D. V. Tunable Hybridization Beetween Electronic States of Graphene and a Metal Surface. *Phys. Rev. B: Condens. Matter Mater. Phys.* **2008**, *77*, 193401.
22. Varykhalov, A.; Sánchez-Barriga, J.; Shikin, A. M.; Biswas, C.; Vescovo, E.; Rybkin, A.; Marchenko, D.; Rader, O. Electronic and Magnetic Properties of Quasifreestanding Graphene on Ni. *Phys. Rev. Lett.* **2008**, *101*, 157601.
23. Usachov, D. Y.; Fedorov, A. V.; Vilkov, O. Y.; Senkovskiy, B. V.; Adamchuk, V. K.; Andryushechkin, B. V.; Vyalikh, D. V. Synthesis and Electronic Structure of Nitrogen-Doped Graphene. *Phys. Solid State* **2013**, *55*, 1325–1332.
24. Bianchini, F.; Patera, L. L.; Peressi, M.; Africh, C.; Comelli, G. Atomic Scale Identification of Coexisting Graphene Structures on Ni(111). *J. Phys. Chem. Lett.* **2014**, *5*, 467–473.
25. Lawlor, J. A.; Ferreira, M. S. Sublattice Asymmetry of Impurity Doping in Graphene: A Review. *Beilstein J. Nanotechnol.* **2014**, *5*, 1210–1217.
26. Zabet-Khosousi, A.; Zhao, L.; Pálová, L.; Hybertsen, M. S.; Reichman, D. R.; Pasupathy, A. N.; Flynn, G. W. Segregation of Sublattice Domains in Nitrogen-Doped Graphene. *J. Am. Chem. Soc.* **2014**, *136*, 1391–1397.
27. Tang, Y.-B.; Yin, L.-C.; Yang, Y.; Bo, X.-H.; Cao, Y.-L.; Wang, H.-E.; Zhang, W.-J.; Bello, I.; Lee, S.-T.; Cheng, H.-M.; *et al.* Tunable Band Gaps and p-Type Transport Properties of Boron-Doped Graphenes by Controllable Ion Doping Using Reactive Microwave Plasma. *ACS Nano* **2012**, *6*, 1970–1978.
28. Varykhalov, A.; Marchenko, D.; Sánchez-Barriga, J.; Scholz, M. R.; Verberck, B.; Trauzettel, B.; Wehling, T. O.; Carbone, C.; Rader, O. Intact Dirac Cones at Broken Sublattice Symmetry: Photoemission Study of Graphene on Ni and Co. *Phys. Rev. X* **2012**, *2*, 041017.
29. Pacilé, D.; Lisi, S.; Di Bernardo, I.; Papagno, M.; Ferrari, L.; Pisarra, M.; Caputo, M.; Mahatha, S. K.; Sheverdyaeva, P. M.; Moras, P.; *et al.* Electronic Structure of Graphene/Co Interfaces. *Phys. Rev. B: Condens. Matter Mater. Phys.* **2014**, *90*, 195446.
30. Usachov, D.; Fedorov, A.; Otrokov, M. M.; Chikina, A.; Vilkov, O.; Petukhov, A.; Rybkin, A. G.; Koroteev, Y. M.; Chulkov, E. V.; Adamchuk, V. K.; *et al.* Observation of Single-Spin Dirac Fermions at the Graphene/Ferromagnet Interface. *Nano Lett.* **2015**, *15*, 2396–2401.
31. Jacobson, P.; Stöger, B.; Garhofer, A.; Parkinson, G. S.; Schmid, M.; Caudillo, R.; Mittendorfer, F.; Redinger, J.; Diebold, U. Disorder and Defect Healing in Graphene on Ni(111). *J. Phys. Chem. Lett.* **2012**, *3*, 136–139.
32. Huang, P. Y.; Ruiz-Vargas, C. S.; van der Zande, A. M.; Whitney, W. S.; Levendorf, M. P.; Kevek, J. W.; Garg, S.; Alden, J. S.; Hustedt, C. J.; Zhu, Y.; *et al.* Grains and Grain Boundaries in Single-Layer Graphene Atomic Patchwork Quilts. *Nature* **2011**, *469*, 389–392.
33. Dzemiantsova, L. V.; Karolak, M.; Lofink, F.; Kubetzka, A.; Sachs, B.; von Bergmann, K.; Hankemeier, S.; Wehling, T. O.; Frömter, R.; Oepen, H. P.; *et al.* Multiscale Magnetic Study of Ni(111) and Graphene on Ni(111). *Phys. Rev. B: Condens. Matter Mater. Phys.* **2011**, *84*, 205431.
34. Zhao, L.; Levendorf, M.; Goncher, S.; Schiros, T.; Pálová, L.; Zabet-Khosousi, A.; Rim, K. T.; Gutiérrez, C.; Nordlund, D.; Jaye, C.; *et al.* Local Atomic and Electronic Structure of Boron Chemical Doping in Monolayer Graphene. *Nano Lett.* **2013**, *13*, 4659–4665.
35. Joucken, F.; Tison, Y.; Lagoute, J.; Dumont, J.; Cabosart, D.; Zheng, B.; Repain, V.; Chacon, C.; Girard, Y.; Botello-Méndez, A. R.; *et al.* Localized State and Charge Transfer in Nitrogen-Doped Graphene. *Phys. Rev. B: Condens. Matter Mater. Phys.* **2012**, *85*, 161408.
36. Zhao, L.; He, R.; Rim, K. T.; Schiros, T.; Kim, K. S.; Zhou, H.; Gutiérrez, C.; Chockalingam, S. P.; Arguello, C. J.; Pálová, L.; *et al.* Visualizing Individual Nitrogen Dopants in Monolayer Graphene. *Science* **2011**, *333*, 999–1003.
37. Wan, W.; Li, H.; Huang, H.; Wong, S. L.; Lv, L.; Gao, Y.; Wee, A. T. S. Incorporating Isolated Molybdenum (Mo) Atoms into Bilayer Epitaxial Graphene on 4H-SiC(0001). *ACS Nano* **2014**, *8*, 970–976.
38. Zheng, B.; Hermet, P.; Henrard, L. Scanning Tunneling Microscopy Simulations of Nitrogen- and Boron-Doped Graphene and Single-Walled Carbon Nanotubes. *ACS Nano* **2010**, *4*, 4165–4173.
39. Garcia-Lekue, A.; Balashov, T.; Olle, M.; Ceballos, G.; Arnau, A.; Gambardella, P.; Sanchez-Portal, D.; Mugarza, A. Spin-Dependent Electron Scattering at Graphene Edges on Ni(111). *Phys. Rev. Lett.* **2014**, *112*, 066802.
40. Vilkov, O.; Fedorov, A.; Usachov, D.; Yashina, L. V.; Generalov, A. V.; Borygina, K.; Verbitskiy, N. I.; Grüneis, A.; Vyalikh, D. V. Controlled Assembly of Graphene-Capped Nickel, Cobalt and Iron Silicides. *Sci. Rep.* **2013**, *3*, 2168.
41. Alimov, V.; Bogomolov, D.; Churaeva, M.; Gorodetsky, A.; Kanashenko, S.; Kanaev, A.; Rybakov, S.; Sharapov, V.; Zakharov, A.; Zalavutdinov, R.; *et al.* Characterization of a-B/C:H Films Deposited From Different Boron Containing Precursors. *J. Nucl. Mater.* **1992**, *196*, 670–675.
42. Grüneis, A.; Kummer, K.; Vyalikh, D. V. Dynamics of Graphene Growth on a Metal Surface: A Time-Dependent Photoemission Study. *New J. Phys.* **2009**, *11*, 073050.